Article

Characterization of a Biodegradable Mg-Alloy after SLM Processing

Doina Raducanu , Vasile Danut Cojocaru , Anna Nocivin * , Silviu Iulian Drob , Radu Emil Hendea , Doina Stanciu , Steliana Ivanescu , Vlad Andrei Raducanu , Nicolae Serban , Elisabeta Mirela Cojocaru , Radu Septimiu Campian

Posted Date: 14 March 2024

doi: 10.20944/preprints202403.0813.v1

Keywords: Mg-alloys; mechanical alloying; selective laser melting; mechanical testing; corrosion resistance

Article

Characterization of a Biodegradable Mg-Alloy after SLM Processing

Doina Raducanu [1], Vasile Danut Cojocaru [1], Anna Nocivin [2,*], Silviu Iulian Drob [3], Radu Emil Hendea [4], Doina Stanciu [5], Steliana Ivanescu [5], Vlad Andrei Raducanu [6], Nicolae Serban [1], Elisabeta Mirela Cojocaru [1] and Radu Septimiu Campian [4]

[1] University POLITEHNICA of Bucharest, Department of Metallic Materials Processing and Ecometallurgy, 060042 Bucharest, Romania; doina.raducanu@upb.ro; dan.cojocaru@upb.ro; nicolae.serban@upb.ro; mirela.cojocaru@upb.ro

[2] OVIDIUS University of Constanta, Faculty of Mechanical, Industrial and Maritime Engineering, 900527 Constanța, Romania; anocivin@univ-ovidius.ro

[3] Romanian Academy, Institute of Physical Chemistry "Ilie Murgulescu", Spl. Independentei 202, 060021 Bucharest, Romania; sidrob.icf@gmail.com

[4] Iuliu Hatieganu University of Medicine and Pharmacy, Faculty of Dental Medicine, Department of Oral Rehabilitation, 400349 Cluj-Napoca, Romania; raduhendea@yahoo.com ; rcampian@email.com

[5] ZIRCON DENT SRL, 400690 Cluj-Napoca, Romania; doinastanciu09@yahoo.com; sivanescu@yahoo.com;

[6] Faculty of Decorative Arts and Design, National University of Arts, 010702 Bucharest, Romania; andrei.raducanu@unarte.org

* Correspondence: anocivin@univ-ovidius.ro

Abstract: A new Mg-Zn-Zr-Ca alloy in powder state was obtained via mechanical alloying method, from pure elemental powder. Further, the obtained powder-alloy was processed by selective laser melting (SLM) procedure to obtain 3D printed samples for small biodegradable implants. A series of microstructural, mechanical and corrosion analysis were performed. The SEM analysis of powder-alloy reveal a good dimensional homogeneity, with uniform colored, no agglutinated and almost rounded particles, suitable for selective laser melting procedure. Further, the SLM samples reveal a robust and unbreakable morphology, with a suitable porosity and without undesirable balling effect. The tested Young's modulus of the SLM samples, of 42 GPa, is close to cortical bone one, of 30 GPa. The corrosion tests performed in PBS (Phosphate-buffered saline) solution show that the corrosion parameters have a satisfactory evolution.

Keywords: Mg-alloys; mechanical alloying; selective laser melting; mechanical testing; corrosion resistance

1. Introduction

Apart from well-known fields of use such as automotive, aerospace and electronics, magnesium alloys are currently widely tested as biomedical components, not only for their high strength-to-weight ratio [1,2], but also for their good structural and mechanical biocompatibility [3,4]. Moreover, in the series of biocompatible materials, magnesium alloys fall under the category of biodegradable materials [5,6], a very useful physical process that prevent a second surgery for removing an anterior inserted bone implant after bone healing due to the fact that magnesium can easily disintegrate in time in human physiological environment [7]. Therefore, if used as temporary orthopaedic implant, novel Mg alloys can replace other bone implants, like Ti-alloys, achieving mechanical performances of human bone by avoiding unwanted stress shielding effects [8–10] and promoting bone remodelling and healing [11–13].

The main advantages of using magnesium alloy as bone implant refers to the fact that it exhibits mechanical performances similar to human bone (low density of 1.74 g/cm^3, and low elastic modulus of about 40-44 GPa, very close to that of cortical bone of 30 GPa, [14]) and, during the degradation in human environment, it represents an essential nutrient which promote bone growth and mineralization [8]. The main disadvantage (unfortunately, there is) is the risk of more rapid

 doi:10.20944/preprints202403.0813.v1

degradation of magnesium alloy, prior to the bone healing process, a fact that require a difficult coordination between the two processes: degradation versus healing [15,16]. Fortunately, the corrosion products that result from the degradation process are non-toxic and can be easily eliminated through the body's metabolism [15]. However, H_2 gas, as a corrosion product, can be accumulated in the surrounding tissue as gas bubbles, causing separation of tissue layers [17,18], and OH^- ions, as another possible corrosion product, can produce surface alkalinization and likely degradation of cells [19]. But in vivo tests showed that the circulation of body fluids facilitates the evacuation of corrosion products that are more abundant in the tissue surrounding the implant in the first period after implantation, and, consequently, the local inflammation is reduced within some days [20,21].

Nowadays, numerous efforts are made to improve the mechanical and biological performances of Mg alloys. One way of action in this direction is the metallurgical optimizing of the chemical composition of the alloy with suitable alloying elements, which allow obtaining microstructures much more adapted to biocompatibility requirements. Another way of action refers to the technological modalities of designing and obtaining a proper bone implant, even a personalized one.

Referring to the chemical composition, the Mg-Zn-Zr alloys (ZK) seem to have superior biocompatibility than already tested Mg-Al-Zn (AZ), or Mg-Zn-RE (WE) [22,23]. Unfortunately, it has been reported that aluminum ions denote a high score for inducing neurotoxicity and brain disorders (Alzheimer's), and, on the other hand, rare elements, as Ce, Y, and Pr, can induce severe hepatotoxicity even if they can reduce the corrosion rate of these alloys [23]. But for ZK alloys, zinc and zirconium, alongside with other possible alloying elements such as Ca, Mn, Si, or Ag, arouse a real interest for the research world due to their high biosafety [24,25]. Thus, zinc, as one possible alloying element for ZK alloys, has an antimicrobial action against bacteria in the implantation area [26], being at the same time an important micronutrient for supporting the immune system and enzymatic reactions [27,28]. On the other hand, zinc is reported to improve the mechanical properties of magnesium alloys, with decreasing their degradation rate and increasing the osteoblastic cells proliferation during bone reconstruction [28]. When the degradation phenomenon of magnesium alloy is occurring, the resulted zinc can be eliminated through the gastrointestinal tract, urine, or skin [29,30]. Biological studies have shown that a zinc content of up to 14.5 (% wt.) is beneficial for the human body, above which an unwanted cytotoxicity of the alloy appears [31]. Zirconium, as other important alloying element, is also a biocompatible one, with low ionic toxicity, improving at the same time the corrosion resistance and mechanical properties of the magnesium alloys, even in small amounts [32]. At the same time, zirconium is bioinert if it is collecting in small amounts in bone or nervous systems [32]. Calcium, in turn, as main mineral of bone components [33], represent another potential and important alloying element to magnesium alloys, with a low density (1.55 g/cm^3) also; research works, as [34,35], report about the exceptional biocompatibility of the binary Mg-Ca alloys. It should also be emphasized that calcium facilitates the hydroxyapatite generation, thereby helping the bone healing [36,37]. Regarding the corrosion resistance of magnesium alloys, calcium, through a controlled composition, can also decrease the corrosion rate, reducing the grain size in the obtained structure [38,39].

Therefore, it would be believed that a promising alternative to the experimental tests carried out so far on ZK ternary alloys (Mg-Zn-Zr) and binary Mg-Ca alloys, would be those that would include all three alloying elements: Zn, Zr and Ca. Thus, the variant selected for study in the present work has alloying elements with compositions that largely converge with those studied so far, being anyway a new one, only reported by the present group of authors. All three alloying elements have a limited solubility in magnesium: zinc, until 6.2% wt. at 340°C [40]; zirconium, until 0.87%wt. at 700°C [41]; calcium, until 1.11% wt. at 521°C [33]. However, in conformity with [7], if the procedure of the alloy obtaining can induce an extent of these solubilities and reach a non-equilibrium supra-saturated solid solution, without secondary phases, the corrosion resistance of the alloy can be evidently improved. Therefore, for the present study a similar/close situation/case was considered when selecting the non-studied before chemical composition: Mg-10Zn-0.8Ca-0.5Zr (%wt.). As a consequence, apart from chemical composition designing, new technological modalities of obtaining

 doi:10.20944/preprints202403.0813.v1

and processing these alloys in a final fabricated bone implant are planned nowadays, even in a personalised design [42,43]. Standard designs of implants are destinated to large groups of patients. However, for helping the surgeon's work to ensure a precise fit for each particular case of patient's bone, in recent years is developing more and more the trend of personalization of the implants using modern 3D printing procedures. For the next five years, the production of personalized 3D printed implants is estimated to reach about 70 billion USD [29].

For the alloy selected for study [Mg-10Zn-0.8Ca-0.5Zr (%wt.)] it has been proposed and used as a method of 3D printing a modern one, named Selective Laser Melting (SLM), a method that can assure for the 3D printed sample/implant the obtaining, beside a personalized shape, some controlled porosities necessary to easily initiate bone regeneration.

The SLM method of additive manufacturing represents a powder bed fusion process which use a high-density laser beam (L-PBF) on a micro scale [44–46]. This method can assure a rapid manufacture of implant metallic parts with custom geometry, without the necessity of post-processing [31,47]. Therefore, a maximum attention should be afforded to the pre-processing step of L-PBF, i.e., the CAD design of the printed model. The final quality of the obtained product is dictated by the selected process parameters, such as the laser power, scanning speed, distance between the printed layers and distance from the hatch. In the case of magnesium and its alloys, which are reactive metallic materials, an inert atmosphere of Argon must be used. To apply the SLM method, the selected alloy must be in powder form, which for this case must be very fine, dense, uniform in size, homogeneous chemically, and as round as possible [48–50]. There are several metallurgical methods for obtaining metal powders. One of the accessible and inexpensive methods is the mechanical alloying process (MA), which involves the milling of pure chemical element powders (≥ 99.00% purity). Using mechanical alloying method, the obtained powder can attempt a nanocrystalline or even amorphous structure because the milling process imply a multitude of severe plastic deformations and provokes repeated fracturing and cold welding of the component particles [51–53].

For the present study, it is proposed a biodegradable alloy, Mg-10Zn-0.8Ca-0.5Zr (% wt.), not tested before by other group of researchers, obtained in a powder state by mechanical alloying, and processed by SLM procedure, in order to obtain a 3D printed sample with adequate microstructural, mechanical and corrosion characteristics suitable for bone implants. Present study represents a complementary research work to anterior published [54,55] papers, which, for this time, is mainly based on mechanical and corrosion analysis, with a summary microstructural analysis.

2. Materials and Methods

- Mechanical Alloying – first applied procedure for obtaining the alloy powder:

To obtain the magnesium alloy in powder form, the mechanical alloying method was applied. The chemical elements selected for alloying the magnesium alloy were: zinc, zirconium and calcium. In order to carry out the mechanical alloying procedure, chemical elements were used in powder form, with a purity of 99.00%, and an average diameter of the powders as follows: Mg < 100 μm, Zn < 40-50 μm, Zr < 40 -50 μm and granules of Ca. The chemical composition calculated to be obtained was: Mg-10Zn-0.8Ca-0.5Zr (%wt.). The amounts of alloying elements were chosen in such a way as to agree with those already reported in the specialized literature and discussed above in the introduction.

The applied mechanical alloying procedure (schema in the Figure 1 - right) involves milling the above powder mixture in the established proportions, using a planetary mill (a PM 100 Retsch type) of high-energy, with a capacity of 500ml and an applied frequency of 50-60Hz.

 doi:10.20944/preprints202403.0813.v1

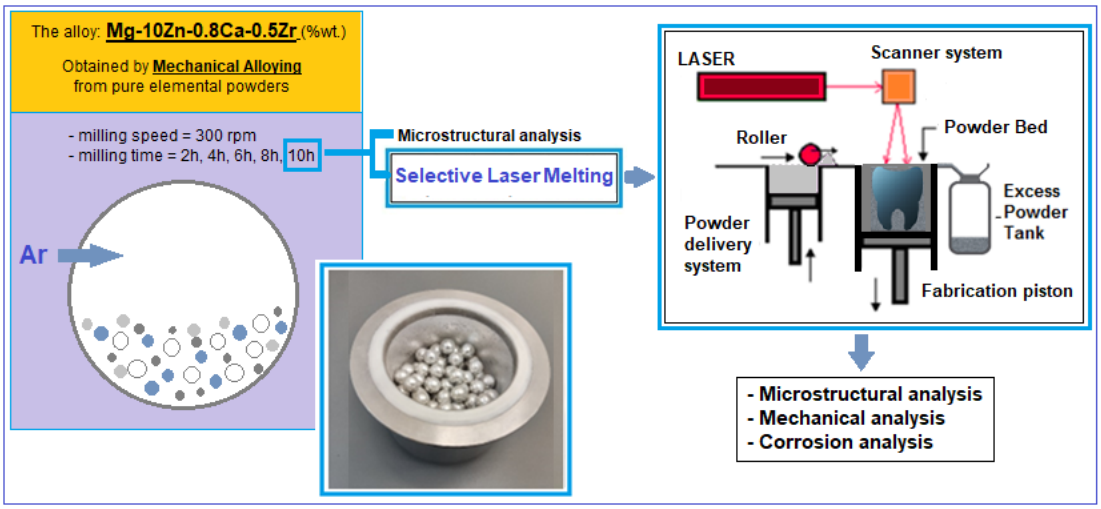

Figure 1. Schema of the experimental program performed for the alloy Mg-10Zn-0.8Ca-0.5Zr (%wt.).

The milling speed is usually applied between 150-350 rpm; for the present case, a value of 300 rpm was applied. To enhance the milling effect, zirconium oxide balls with a diameter of approx. 10mm, with a weight ratio of 10:1 are added to the powder mixture. For oxidation protection, the argon atmosphere of 1.5 bar overpressure is used. Also, during milling process cold welding of the powder particles can occur; to prevent this phenomenon, 5% n-heptane solution was added. For the present experimental test, the variable parameter was the milling time. Increasing times from two-to-two hours were tested, starting from 2h to 10h. The objective was to finally obtain a powder-alloy with a chemical composition and a microstructure as homogeneous and consistent as possible. Therefore, the milling time was extended as much as possible.

After mechanical alloying procedure, the obtained powder-alloy was subjected to a sieving operation with smaller and smaller dimensions; the final one was < 30 μm.

- Selective Laser Melting (SLM) – second applied procedure for obtaining a bulk specimen from the alloy powder

The finest powder obtained after mechanical alloying was subjected to 3D printing processing by SLM method (schema in the Figure 1 - left).

For that, the laser used was of MYSINT 100-3D Selective Laser Fusion type (SISMA s.p.a., Vicenza, Italy), that is a laser special dedicated to printing metallic powder. The applied parameters were: the power supply of 220-240 V with 50/60Hz; the absorbed maximum power of 1.53 kW; laser power – 40-150W; laser speed – 300-1000 mm/s; layer height – 20-30 μm; laser energy density – 100-550 J/mm^3; as inert gas, Nitrogen and Argon were used. Several samples with dimensions of 10x10x12 mm (Length x Width x Height) were obtained in order to be tested forward to SEM analysis (one sample), compression test (nine samples), and corrosion test (three samples).

- Microstructural and Mechanical analysis of the studied Mg-alloy processed by SLM

The microstructural analysis of the Mg-Zn-Ca-Zr alloy (in powder state and after SLM processing) started with a SEM-SE (Scanning electron microscopy–secondary electron) imaging investigation, that was performed on a Tescan VEGA II-XMU SEM microscope (Tescan Orsay Holding a.s. Brno, Czech Republic). Concomitant, calculations of powder characteristics, such as dimension, morphology and homogeneity, were made. The XRD analysis was performed at room temperature (RIGAKU MiniFlex600, Tokyo, Japan) using Cu-Kα radiation with a scattering angle 2θ in the range of 30-90 degrees for a step size of 0.02 degrees. Nine samples of the studied Mg-Zn-Ca-Zr alloy, after SLM printing procedure, were subjected to the compression test. For that, it has been used a universal testing machine of INSTRON 3382 type (Instron Ltd., High Wycombe, Buckinghamshire, HP123SY, UK). The samples were subjected to a constantly increasing loads until they finally broke.

 doi:10.20944/preprints202403.0813.v1

- Corrosion analysis of the studied Mg-alloy processed by SLM

The corrosion monitoring was carried out using a potentiostat (Radiometer Analytical VoltaLab PGZ 402, France). Thus, three corrosion tests were conducted: open circuit potential, impedance (EIS), using a value of 200mV, and polarisation for corrosion (Tafel plots) [56]. The polarisation for corrosion test was conducted using a range from -1600mV to +1600mV, using also a scan speed of 2mV/s; as a result, the potentiostat's software (VoltaMaster 4, version 7.9) provided the following data, using a preset calculation method (1st Stern method: Tafel): the corrosion rate (V_{corr}), the corrosion current (i_{corr}), the polarization resistance (R_p), the electrode potential ($E_{(i=o)}$), and the anodic and cathodic Tafel constants (β_a & β_c). Tests were performed in triplicate.

3. Results and Discussions

3.1. Microstructural Characterization of the Mg-Zn-Ca-Zr Alloy in Powder State and after SLM Processing

As already stated in the introduction, in the previously published articles [54,55] the preponderance was the microstructural analysis of the studied alloy. In the article [54], the emphasis was placed on the step-by-step follow-up of the morphological and compositional evolution of the powder-alloy obtained through mechanical alloying by varying the milling time. In the second article [55], the microstructural evolution of the subsequent 3D printed samples using the SLM method by varying the Laser energy density parameter was highlighted. The present work tries to take a step forward by deepening the research regarding the mechanical behavior of the same alloy processed by SLM as well as the corrosion resistance of this alloy. Thus, the microstructural analysis was performed this time only on the samples proving previous best suitable results: first, on powder alloy obtained by mechanical alloying with a milling time of 10 h, and then after SLM processing with Laser energy density (E) having the value of 134 J/mm^3 and a scanning speed of 600 mm/s, as two parameters with higher influence.

Figure 2 shows two representative SEM images obtained after microscopic analysis of the studied Mg-Zn-Ca-Zr alloy in powder state, as it has been resulted after mechanical alloying procedure with a milling time of 10h. Looking at the powder morphology, several important features were observed using a SEM calibrated microscope.

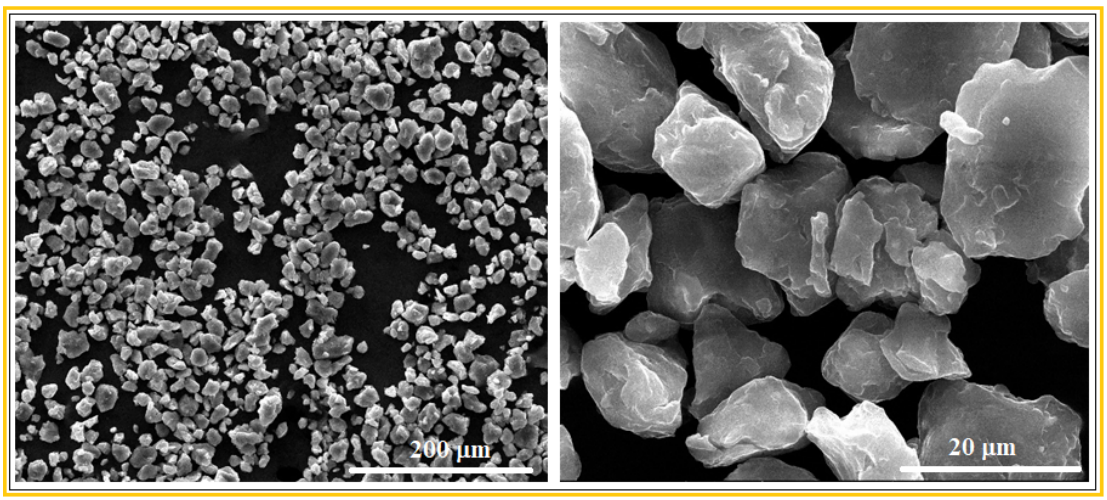

Figure 2. The SEM-SE images for the Mg-Zn-Ca-Zr (%wt.) powder-alloy after mechanical alloying with a milling time of 10h.

First, it is a dimensional homogeneity of the powder particles with an average value of 16.2 ± 8.6 µm. In conformity with *[42–44]*, this average dimension is satisfactory for the subsequent SLM procedure.

 doi:10.20944/preprints202403.0813.v1

A second important characteristic refers to the surface of the powder particles that looks to be homogeneous, with a uniform colour and without signs of inhomogeneities; the structure is formed from a single phase with alloying elements fully solubilized in magnesium, and, consequently, without secondary phases. Moreover, the lack of secondary phases and the complete solubilization of the alloying elements was also proven by XRD analysis (Figure 3), which indicates patterns corresponding to the magnesium-based solid solution, α-Mg. Having in view that for the present case the amount of zinc exceeds the limit of solubility in Mg (6.2 %wt.), if the synthesis procedure had followed the classic line of alloy obtaining (melting-solidification) then the secondary phase $MgZn_2$ should have been formed. Unlike the classic version, during the mechanical alloying procedure there are severe plastic deformations of the powder particles, accompanied by cold welding and their strong and constant fractures, which give rise to a strong energy that can lead to a homogeneous distribution of the chemical elements in the Mg powder particles. There are works, such as [57], which clearly confirm this possibility, and even for the extreme case where the amorphous structure can be obtained [58] at much longer milling times, about 70h and more. In the present case, the total absence of $MgZn_2$ in the XRD patterns cannot be absolutely guaranteed for the real structure, considering the possible minute amount of precipitate formed, and the low sensitivity of the device used.

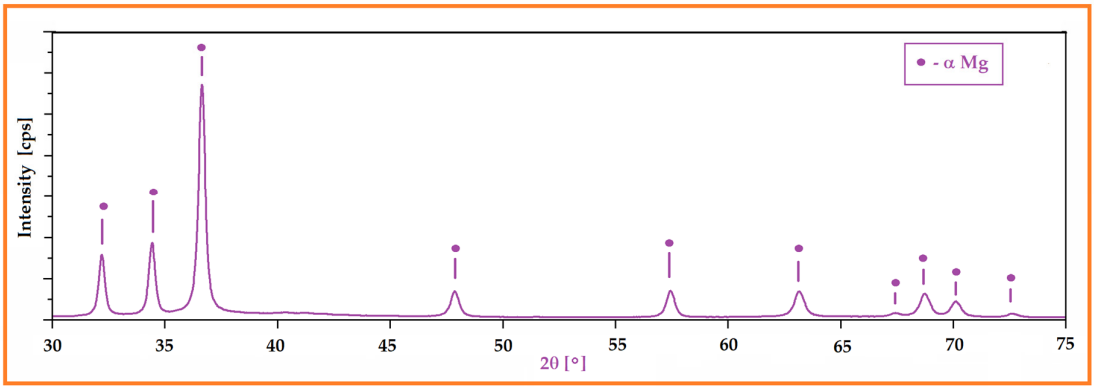

Figure 3. The XRD spectra of the Mg-Zn-Ca-Zr (%wt.) powder-alloy after mechanical alloying with a milling time of 10h.

Finally, another positive morphological characteristic observed was that, unlike the shorter milling times, at 10h no agglutinated particles were observed, having an individualized appearance, with regular, smooth and relatively rounded shapes, if compared with smaller milling times with sharper shapes. Therefore, all these particular characteristics can be considered to have been suitable for the subsequent SLM process for which, in general, a fine powder with homogeneous and almost rounded shapes is required.

Figure 4 shows some representative SEM images obtained by microscopic analysis of the Mg-Zn-Ca-Zr alloy, after SLM procedure. The initial macroscopic examination of the obtained SLM samples of 10x10x12 mm shows a robust state, but relatively porous and without cracks that correspond to the proposed objective – to obtain a structure that can reproduce the cortical bone one.

In that sense, the examination by SEM analysis was made inside of the SLM samples, in order to observe the homogeneous distribution of the robustness and porosity, cumulative, in the entire volume of the samples. From the SEM images corresponding to Figure 4, it can be seen that the examined surfaces, exposed at a gradually increasing magnification, show a dense and unbreakable morphology, without the balling effect known to be detrimental to the mechanical performance and therefore undesirable.

 doi:10.20944/preprints202403.0813.v1

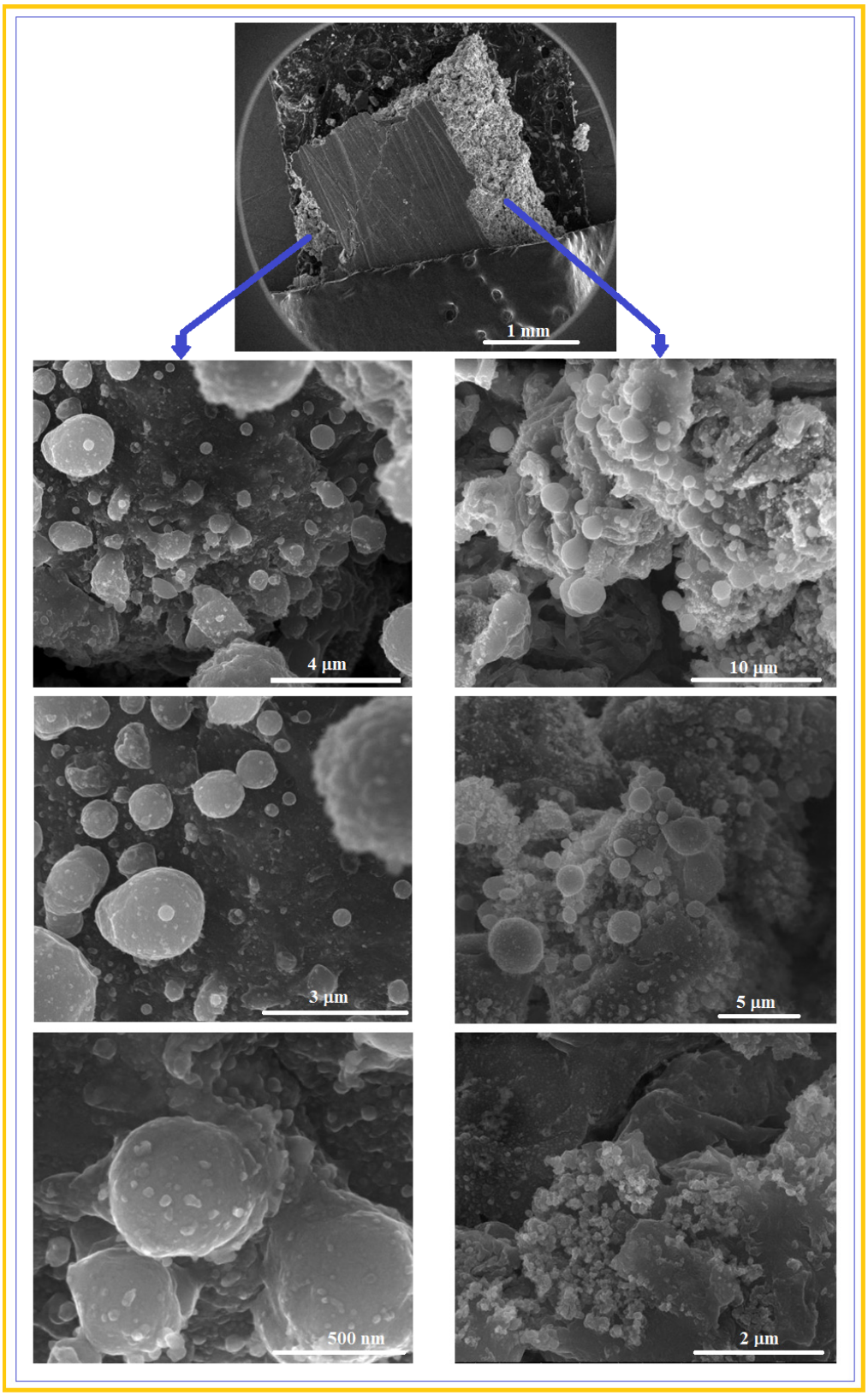

Figure 4. The SEM-SE images for the Mg-Zn-Ca-Zr (%wt.) alloy after selective laser melting – SLM processing.

 doi:10.20944/preprints202403.0813.v1

The degree of porosity obtained by the SLM procedure must be correlated with a real and therefore desired level of cortical bone porosity. This "desired" level can be set/standardized depending on the type and location of the bone implant and can be achieved by a judicious selection of the SLM processing parameters. However, for the present case, the SLM samples, judging by their morphological condition, can be considered suitable for an early examination of their mechanical and corrosion performance.

3.1. Mechanical Characterization of the Mg-Zn-Ca-Zr Alloy in Powder State and after SLM Processing

Compression tests were applied for a set of nine samples realized by SLM processing. Figure 5 shows the dimensional aspect of some samples, before and after testing. The strain–stress curves for each of all nine tested samples are presented all together in Figure 6. After processing the data resulted from these curves, the determination of the mechanical characteristics was made for all tested samples. Thus, Figure 7 shows the representative strain–stress curve resulted by weighting the data from all tested samples and Table 1 shows the average corresponding values for: maximum compressive strength (σ_{max}); deformation to fracture (ε_{max}) and elastic modulus (E). Standard deviation was calculated and has been included in Table 1.

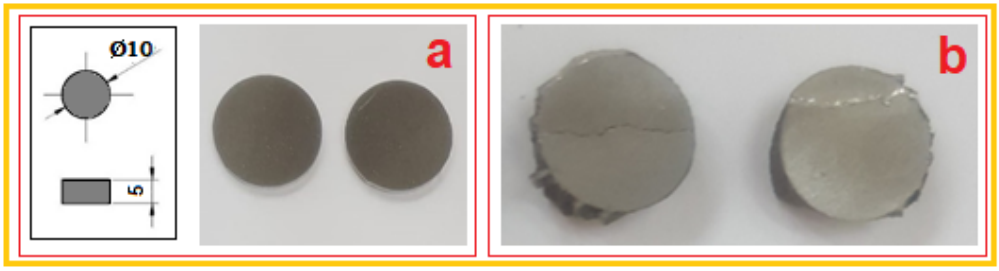

Figure 5. SLM samples before (a) and after (b) compression test.

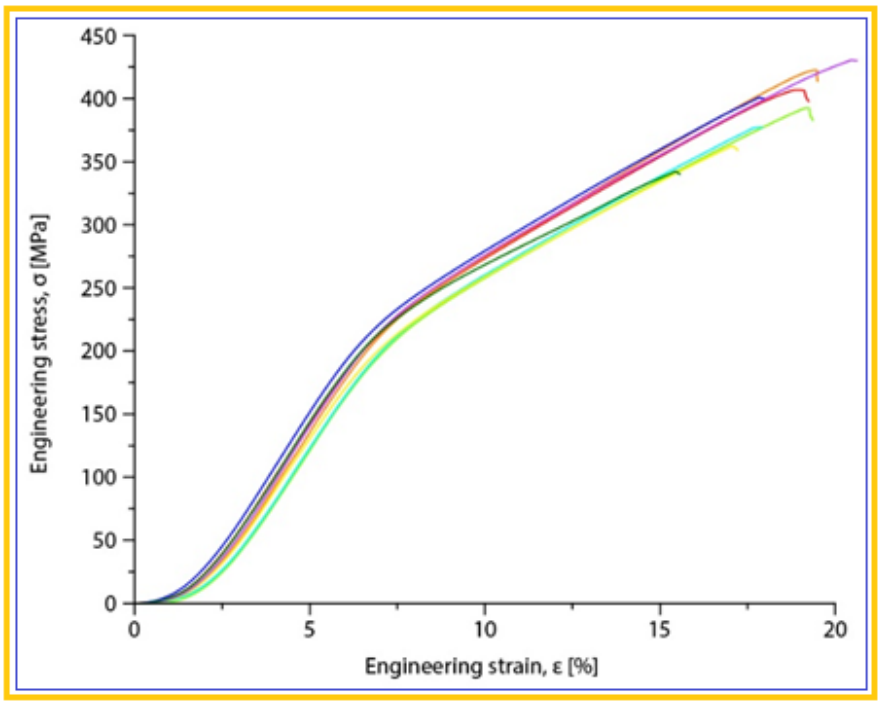

Figure 6. Stress- strain diagrams for the nine SLM samples tested at compression test.

 doi:10.20944/preprints202403.0813.v1

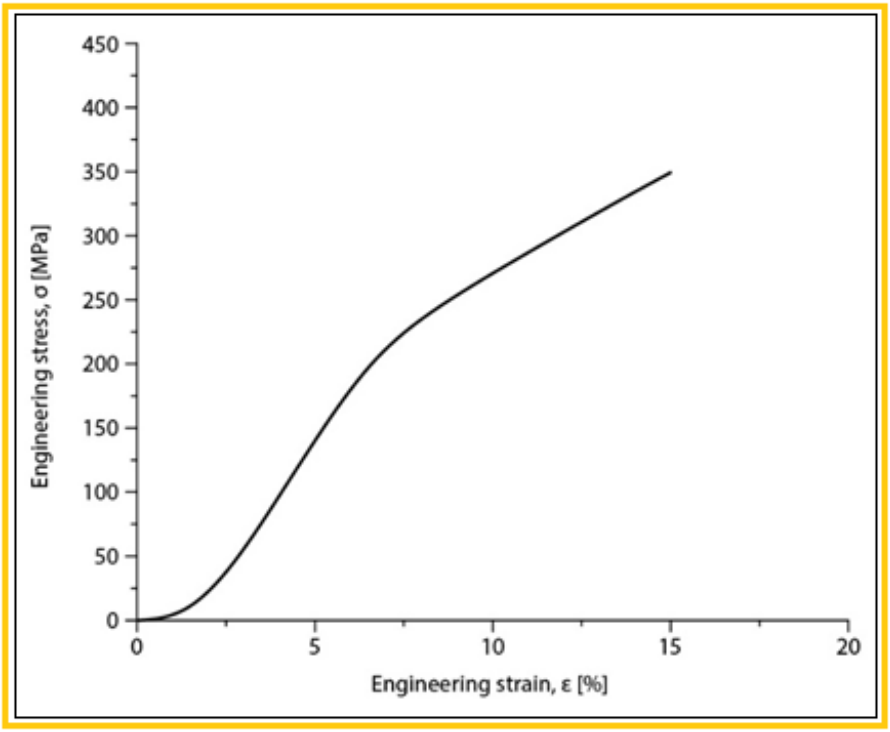

Figure 7. Stress-strain diagram for the Mg-Zn-Ca-Zr (%wt.) alloy in SLM condition after compression test.

Table 1. Mechanical properties of the studied alloy after SLM processing : Ultimate Compressive Strength (σ_{max}); Deformation to Fracture (ε_{max}); Elastic Modulus (E); SD (Standard Deviation).

The alloy in SLM condition	σ_{max} [MPa]	ε_{max} [%]	E [GPa]
Mg-10Zn-0.8Ca-0.5Zr (%wt.)	381.25±17.19	17.92±0.44	42.10±1.08

Examining the data in Table 1, it can be said that the values obtained for the main mechanical properties are generally close to those of cortical bone [8,9], especially for the Young modulus (30 GPa for cortical bone comparative to 42 GPa for the tested samples), which means that, for an implant made of this alloy and using SLM technology that ensures a certain desired porosity of the material, the risk of the stress-shielding phenomenon is very low, especially if this type of implant is designed to be biodegradable in due time.

3.1. Corrosion Analysis of the SLM Processed Mg-Based Alloy.

For the corrosion test, three samples of studied Mg-alloy after 3D printing by SLM procedure were used. These three samples were tested in PBS (Phosphate-buffered saline) solution with 3 different pH values (based on Roth Roti®CELL PBS CELLPURE®), with the intention of covering the widest possible range of pH variation in the human body: (1) Stock PBS [59] solution with a pH of 7.4; (2) HCl (0.1M) doped PBS with a pH of 3.16 and (3) KOH (pellets) doped PBS with a pH of 10.1. All tests were conducted using SCE (Hg/Hg_2Cl_2 – Sat. KCl) Ag/AgCl (3M KCl) as a reference electrode, a Pt wire electrode as counter electrode, and the samples as the working electrode. For each pH, three different immersion times were tested: 0 h, 24 h and 48 h. During all performed tests, an important amount of hydrogen emission was observed – Figure 8. After the corrosion tests were concluded, each of three electrochemical cells were stored in a digital drying oven at 37°C.

 doi:10.20944/preprints202403.0813.v1

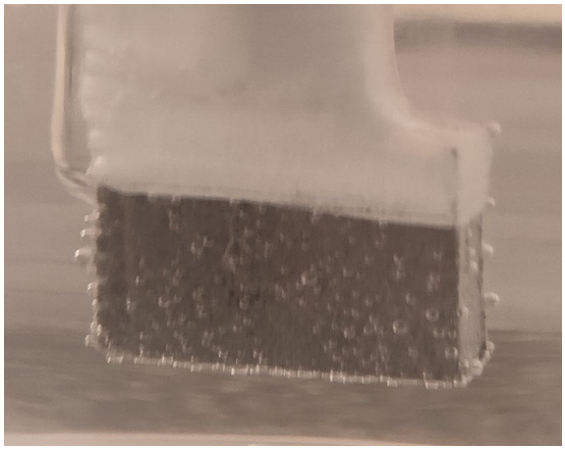

Figure 8. Hydrogen bubbles release on the surface of the working electrode (sample).

Figures 9–11 show the Nyquist spectra and Tafel spectra obtained for the tested samples. The resulting Nyquist spectra have a convulsing/trembling shape due to the noise generated by the massive amounts of hydrogen release. These hydrogen bubbles adhered to the surface of the sample and, as such, interfered with the readings during the tests performed as seen in Figure 8. The generation of hydrogen, inevitable in the case of magnesium alloys, can create a considerable variability of the results, unfortunately; this situation can be augmented, in addition, by the high roughness of the surface of the SLM samples, a sine-qua-non condition by the way, by which the generation of hydrogen is higher than in the case of more compact surfaces of the samples. This roughness is assumed in this case, out of the desire to imitate the more porous surface of the cortical bone that will support joining with a biodegradable implant made of such a magnesium alloy. Being an accelerated corrosion test, finally, all samples were dissolved and formed a dark grey precipitate on the bottom of their respective electrochemical cells.

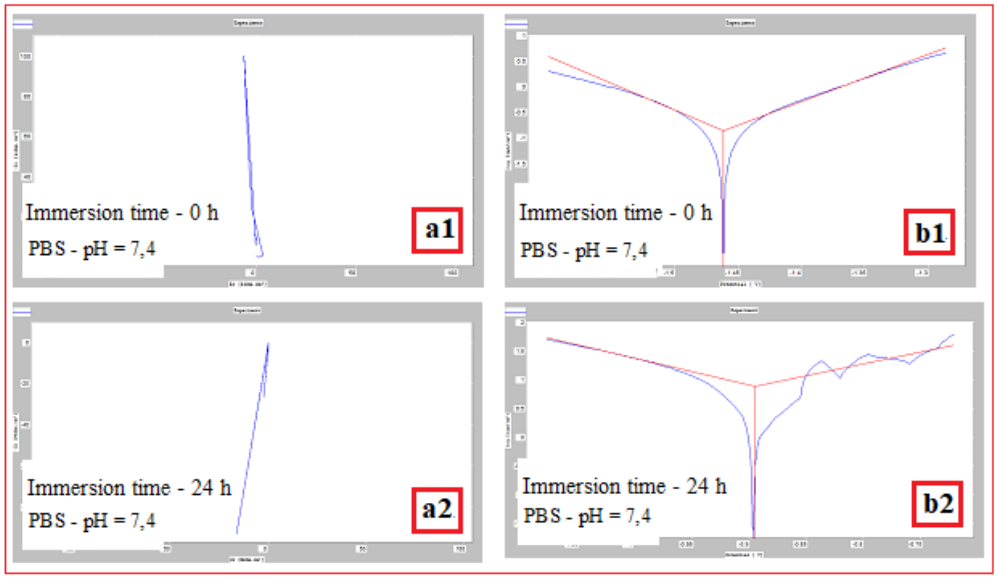

Figure 9. Nyquist spectra (a1, a2) and Tafel spectra (b1, b2) for the SLM sample tested in PBS with pH 7,4, at immersion times of 0 h and 24 h.

 doi:10.20944/preprints202403.0813.v1

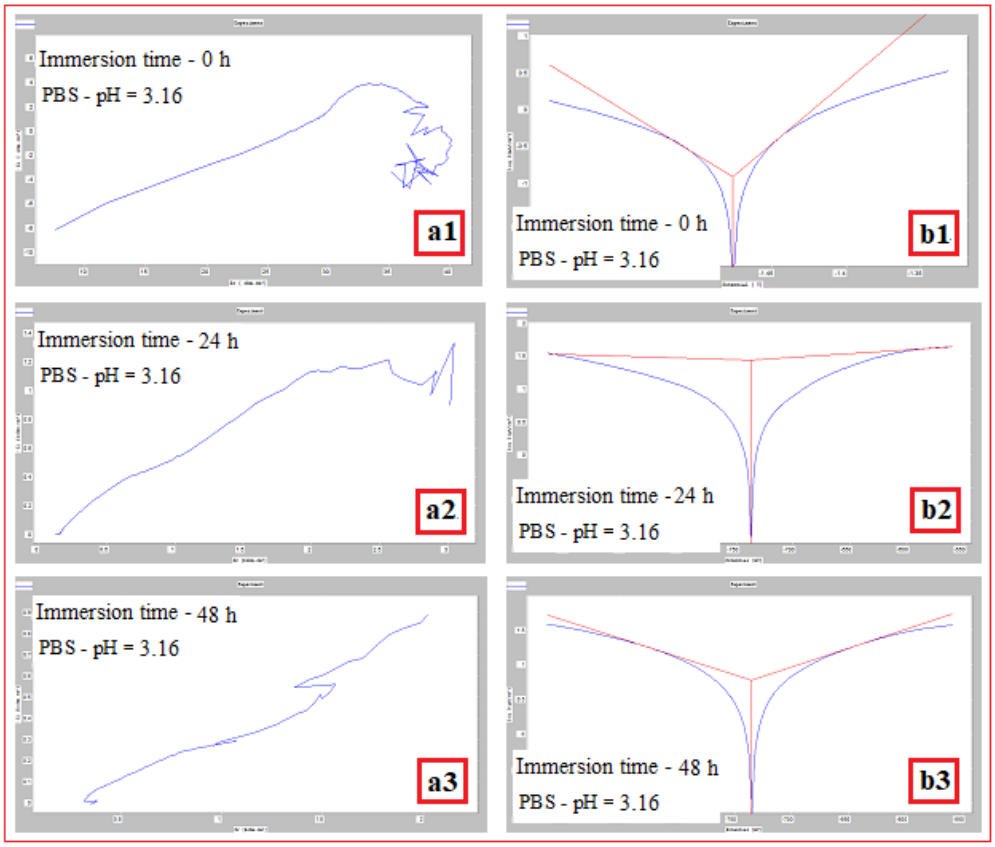

Figure 10. Nyquist spectra (a1, a2, a3) and Tafel spectra (b1, b2, b3) for SLM sample tested in PBS with pH 3.16, at immersion times of 0 h, 24 h and 48 h.

 doi:10.20944/preprints202403.0813.v1

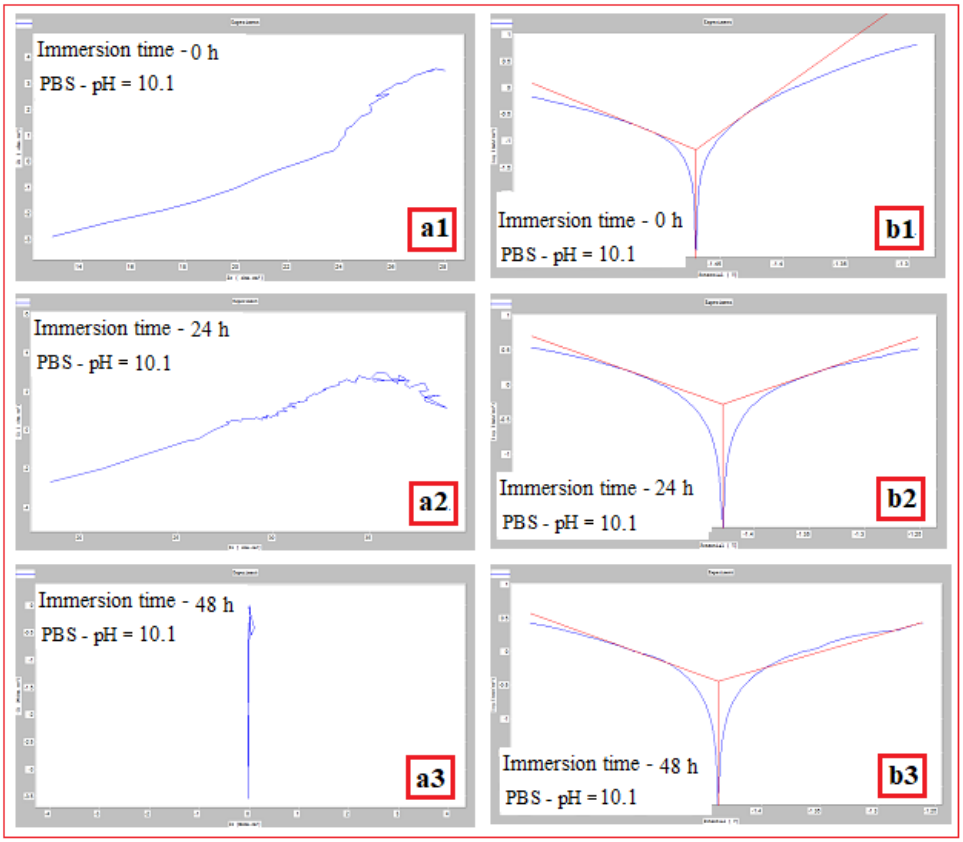

Figure 11. Nyquist spectra (a1, a2, a3) and Tafel spectra (b1, b2, b3) for SLM sample tested in PBS with pH 10.1, at immersion times of 0 h, 24 h and 48 h.

The main parameters determined, which resulted from these corrosion analyses, are shown in Table 2: the corrosion current (j_{corr}), the electrode potential ($E_{(i=o)}$) and the corrosion rate (V_{corr}). The resulting corrosion rate values for each tested sample, are indicated in the Figure 12.

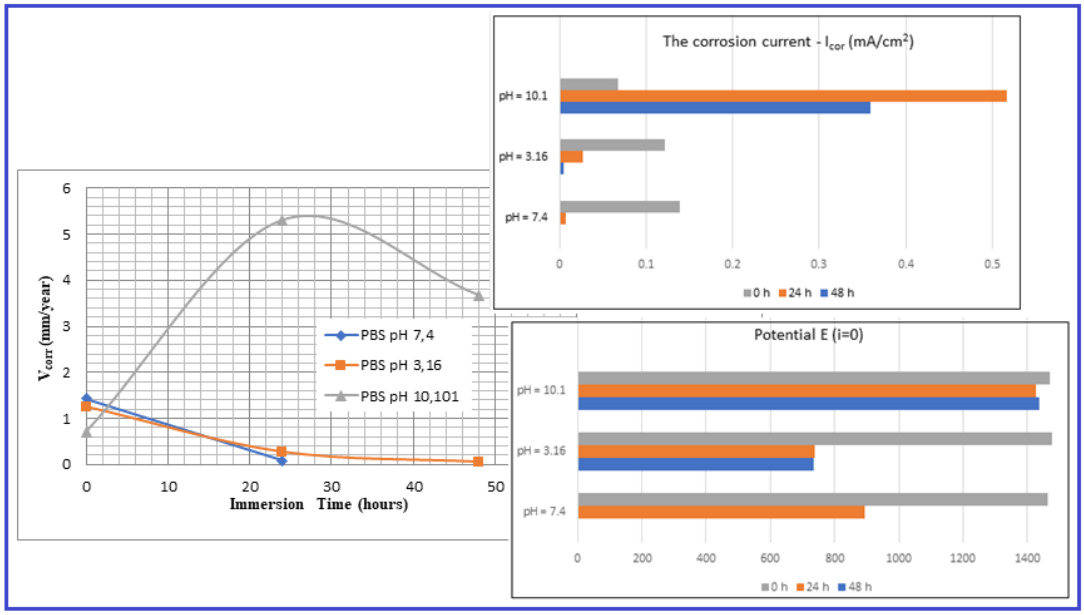

 doi:10.20944/preprints202403.0813.v1

Figure 12. The evolution of the corrosion rate for the tested samples.

Table 2. Main corrosion parameters for tested SLM samples in PBS solution, with three different pH values and different immersion times.

Mg-alloy, SLM processed, Immersed in PBS with pH:	**Immersion time (h)**	**V_{cor} (mm/year)**	**I_{cor} (mA/cm²)**	**Potential E(i=o) (mV)**
pH = 7,4	0	1,426±0.04	0,139±0.026	-1462,1±2.1
	24	0,079±0.01	0,007±0.001	-895±1.3
	48	-	-	-
pH = 3,16	0	1,252±0.04	0,122±0.016	-1476,4±2.1
	24	0,278±0.02	0,027±0.004	-737,9±1.1
	48	0,060±0.01	0,005±0.001	-735±1.1
pH = 10,1	0	0,703±0.06	0,068±0.002	-1469,6±2.8
	24	5,305±0.12	0,517±0.022	-1428±2.2
	48	3,679±0.10	0,359±0.013	-1437,6±2.4

For increasing the corrosion performance of a metallic alloy, it was generally established that the electrode potential must have an upward trend (should be high), and the corrosion current must be low *[60–62]*. This fact can be seen from the values of Table 2. A similarity of the corrosion parameters evolution can be seen for both neutral and acidic pH. If compare these values with those corresponding to the commercial ZK60 alloy (around 1.45 mm/year *[63–68]*), it can be found that the obtained here values can be considered quite satisfactory.

For basic pH (10.1), however, notable differences are observed: the electrode potential and the current density have a fluctuating variation (increase/decrease), and the resulting corrosion rates are outside the ranges generally reported. This fact is highlighted by Figure 12 also. These types of inadvertences can probably be attributed to the fact that hydrogen release was not counted. It should be pointed out that the PBS solution with a basic pH (10.1) represents an experimental situation and not a real phisiologic test as for real regular implants. However, the alkalization can occur in the case of Mg-based implants, reaching a pH level of ten and even higher [69]. Moreover, in conformity to [7], it seems that the corrosion rate can be substantially improved by expanding the solubility of the alloying elements using non-equilibrium techniques, without causing the serious micro-galvanic corrosion that usually is generated when the added alloying elements precipitate as second phase particles. The mechanical alloying procedure, used for present experimental program, can be considered a non-equilibrium technique because the amount of zinc exceeds the limit of solubility in Mg (10%wt. instead of 6.2 %wt.) through severe plastic deformations that occur durring the process.

However, as a good result noted from these experiments, it should be mentioned and emphasized that at neutral pH, the corrosion rate of the Mg-10Zn-0.8Ca-0.5Zr alloy (1.426 mm/year) is very close to that of the alloy considered as a etalon for comparing nowadays - ZK 60 (1.45 mm/year) [63–68].

5. Conclusions

- A magnesium alloy with the composition of Mg-10Zn-0.8Ca-0.5Zr (%wt.) has been obtained via mechanical alloying using pure elemental powders. After 10h of milling in argon atmosphere, the obtained powder alloy reveals a uniform dimensional homogeneity with an average particle size of 16.2 ± 8.6 μm and no agglutinated particles. The powder particles have also a homogeneous microstructure, with a uniform colour and no agglutinated particles. This powder alloy has been processed by 3D printing, using the SLM method.

- The SEM microstructural analysis of the SLM samples reveal a dense and unbreakable morphology, but with a suitable porosity and without undesirable balling effect.

 doi:10.20944/preprints202403.0813.v1

- After compression test, the alloy samples in SLM condition have a Young's modulus of 42 GPa, close to the cortical bone one, of 30 GPa, avoiding the stress shielding effect.

- The SLM samples tested for corrosion resistance in PBS solution with 3 different pH values show that the corrosion parameters have a satisfactory evolution. At the normal neutral body pH, the corrosion rate of Mg-10Zn-0.8Ca-0.5Zr alloy (1.426 mm/year) is very close to that of ZK 60 alloy (1.45 mm/year).

Author Contributions: Conceptualization, D.R.; A.N.; V.D.C.; methodology, R.E.H.; software, V.A.R.; S.I.D.; validation, D.R.; A.N.; V.D.C.; formal analysis, D.R.; investigation, D.S.; S.I.; N.S.; V.A.R.; E.M.C.; R.S.C.; resources, V.D.C.; data curation, S.I.D.; writing—original draft preparation, A.N.; D.S.; writing—review and editing, A.N.; D.R.; visualization, D.R.; A.N.; V.D.C.; supervision, D.R.; A.N.; project administration, D.R.; V.D.C.; funding acquisition, D.R.; V.D.C. All authors have read and agreed to the published version of the manuscript.

Funding: This research was funded by Romanian National Authority for Scientific Research, CCCDI – UEFISCDI, Project ERANET-MANUNET-AMMBI/grant no. 207/2020.

Institutional Review Board Statement: Not applicable.

Informed Consent Statement: Not applicable.

Data Availability Statement: The data presented in this study are available on request from the corresponding author.

Acknowledgments: The authors acknowledge financial support for this research by the Romanian National Authority for Scientific Research CCCDI–UEFISCDI, Project ERANET-MANUNET-AMMBI/grant no. 207/2020.

Conflicts of Interest: The authors declare no conflict of interest.

References

1. Esmaily M., Svensson J.E., Fajardo S., Birbilis N., Frankel G.S., Virtanen S., Arrabal R., Thomas S., Johansson L.G., Fundamentals and advances in magnesium alloy corrosion, *Prog. Mater. Sci*., **2017**, 89, 92-193, https://doi.org/10.1016/j.pmatsci.2017.04.011
2. Song J., She J., Chen D., Pan F., Latest research advances on magnesium and magnesium alloys worldwide, *J. Magnes. Alloy*, **2020**, 8(1), 1-41, https://doi.org/10.1016/j.jma.2020.02.003
3. Lovašiová, P.; Lovaši, T.; Kubásek, J.; Jablonská, E.; Msallamová, Š.; Michalcová, A.; Vojtˇech, D.; Suchý, J.; Koutný, D.; Ghassan Hamed Alzubi, E. Biodegradable WE43 Magnesium Alloy Produced by Selective Laser Melting: Mechanical Properties, Corrosion Behavior, and In-Vitro Cytotoxicity. *Metals* **2022**, 12, 469.
4. Chen X., Ning S., Wang A., Le Q., Liao Q., Jia Y., Cheng C., Li X., Atrens A., Yu F., Microstructure, mechanical properties and corrosion behavior of quasicrystal-reinforced Mg-Zn-Y alloy subjected to dual-frequency ultrasonic field, *Corros. Sci*., **2020**, 163, Article 108289, https://doi.org/10.1016/j.corsci.2019.108289
5. Zhang J., Zhang B., Zhang J., Lin W., Zhang S., Magnesium promotes the regeneration of the peripheral nerve; *Front. Cell Dev. Biol.,* **2021**, 2169, 717854, https://doi.org/10.3389/fcell.2021.717854
6. Dong J., Lin T., Shao H., Wang H., Wang X., Song K., et al., Advances in degradation behavior of biomedical magnesium alloys: A review. *J. Alloys Compd*. **2022**, 908, 164600. https://doi.org/10.1016/j.jallcom.2022.164600
7. Cao F., Xiao B., Wang Z., Ying T., Zheng D., Atrens A., Song G.-L., A Mg alloy with no hydrogen evolution during dissolution, *J. Magnes. Alloys*, **2023**, 11(6), 2084-2095, https://doi.org/10.1016/j.jma.2021.08.024
8. Li W., Qiao W., Liu X., Bian D., Shen D., Zheng Y., et al., Biomimicking bone-implant interface facilitates the bioadaption of a new degradable magnesium alloy to the bone tissue microenvironement. *Adv. Sci.* **2021**, 8, 2102035, https://doi.org/10.1002/advs.202102035
9. Amukarimi S., Mozafari M., Biodegradable magnesium-based biomaterials: An overview of challenges and opportunities. *MedComm,* **2021**, 2, 123-144, https://doi.org/10.1002/mco2.59
10. Banerjee P., Saadi S., Choudhary L., Harandi S.E., Singh R., Magnesium implants: Prospects and challenges. *Materials*, **2019**, 12, 136, https://doi.org/10.3390/ma12010136
11. O'Neill E., Awale G., Daneshmandi L., Umerah O., Lo K.W.H., The roles of ions on bone regeneration, *Drug Discov. Today*, **2018**, 23, 879-890, https://doi.org/10.1016/j.drudis.2018.01.049
12. Qin Y., Wen P., Guo H., Xia D., Zheng Y., Jauer L., et al., Additive manufacturing of biodegradable metals: Current research status and future perspectives. *Acta Biomater*. **2019**, 98, 3-22, https://doi.org/10.1016/j.actbio.2019.04.046

13. Zhou H., Liang B., Jiang H., Deng Z., Yu K., Magnesium based biomaterials as emerging agents for bone repair and regeneration: From mechanism to application. *J. Magnes. Alloys*, **2021**, 9, 779-804, https://doi.org/10.1016/j.jma.2021.03.004
14. Ting Zhang, Wen Wang, Jia Liu, Liqiang Wang, Yujin Tang, Kuaishe Wang, A review on magnesium alloys for biomedical applications, *Front. Bioeng. Biotechnol*., 16 August **2022**, Sec. Biomaterials, Vol. 10-2022, https://doi.org/10.3389/fbioe.2022.953344
15. Wang J.L., Xu J.K., Hopkins C., Chow D.H.K., Qin L., Biodegradable magnesium based implants in orthopedics – A general review and perspectives. *Adv. Sci.* **2020**, 7, 1902443, https://doi.org/10.1002/advs.201902443
16. Wang W., Han P., Peng P., Zhang T., Liu Q., Yuan S.-N., et al., Friction stir processing of magnesium alloys: A review, *Acta Metall. Sinica (Eng Letters)*, **2020**, 33(1), 43-57, https://doi.org/10.1007/s40195-019-00971-7
17. Jung O., Porchetta D., Schroeder M.-L., Klein M., Wegner N., Walther F., et al., In vivo simulation of magnesium degradability using a new fluid dynamic bench testing approach. *Int. J. Mol. Sci*. **2019**, 20, 4859. https://doi.org/10.3390/ijms20194859
18. Kumar K., Gill R., Batra U., Challenges and opportunities for biodegradable magnesium alloy implants. *Mat. Technol. (N.Y.N.Y.)* **2018**, 33, 153-172, https://doi.org/10.1080/10667857.2017.1377973
19. Chin, P., Cheok, Q., Glowacz, A., and Caesarendra, W., A review of in-vivo and in-vitro real-time corrosion monitoring systems of biodegradable metal implants, *Appl. Sci.* (Basel), **2020**, 10(9), 3141, https://doi.org/10.3390/app10093141
20. Kim Y.K.; Lee K.B.; Kim S.Y.; Bode K.; Jang Y.S.; Kwon T.Y.; Jeon M.H.; Lee M.H.; Gas formation and biological effects of biodegradable magnesium in a preclinical and clinical observation, *Sci. Technol. Adv. Mater*., **2018**, 19:1, 324 – 335, DOI: 10.1080/14686996.2018.1451717
21. Kuhlmann J., Bartsch, Willbold E.; Schuchardt S.; Holz O.; Hort N.; Höche D.; Heineman W.R.; Witte F.; Fast escape of hydrogen from gas cavities around corroding magnesium implants, *Acta Biomaterialia*, **2013**, 9(10), 8714-8721, https://doi.org/10.1016/j.actbio.2012.10.008
22. Huan, Z.G.; Leeflang, M.A.; Zhou, J.; Fratila-Apachitei, L.E.; Duszczyk, J. In vitro degradation behavior and cytocompatibility of Mg–Zn–Zr alloys. *J. Mater. Sci.Mater. Med*. **2010**, 21, 2623–2635.
23. Gu, X.; Xie, X.; Li, N.; Zheng, Y. In vitro and in vivo studies on a Mg–Sr binary alloy system developed as a new kind of biodegradable metal. *Acta Biomater*. **2012**, 8, 2360–2374.
24. Seifen, S.; Hock, M. Development of magnesium implants by application of conjoint-based quality function deployment. *J. Biomed. Mater. Res*. **2019**, 107, 2814–2834.
25. Shuai, C.; Zhou, Y.; Yang, Y.; Gao, C.; Peng, S.; Wang, G. Ag-Introduced Antibacterial Ability and Corrosion Resistance for Bio-Mg Alloys. *BioMed Res. Int*. **2018**, 6023460.
26. Seetharaman, S.; Sankaranarayanan, D.; Gupta, M. Magnesium-Based Temporary Implants: Potential, Current Status, Applications, and Challenges. *J. Funct. Biomater*. **2023**, 14, 324.
27. Li, X.; Liu, X.; Wu, S.; Yeung, K.; Zheng, Y.; Chu, P.K. Design of magnesium alloys with controllable degradation for biomedical implants: From bulk to surface. *Acta Biomater*. **2016**, 45, 2–30.
28. Sezer, N.; Evis, Z.; Kayhan, S.M.; Tahmasebifar, A.; Koça, M. Review of magnesium-based biomaterials and their applications. *J. Magnes. Alloys* **2018**, 6, 23–43.
29. Global Personalized 3D Printed Orthopedic Implants Market, Data Bridge Market Research. Available online: https://www. databridgemarketresearch.com/reports/global-personalized-3d-printed-orthopedic-implants-market (accessed on 8 December 2023).
30. Roohani, N.; Hurrell, R.; Kelishadi, R.; Schulin, R. Zinc and its importance for human health: An integrative review. J. Res. Med. Sci. 2013, 18, 144–157. Available online: https://www.researchgate.net/publication/27120142 (accessed on 16 December 2023)
31. Zhang, M.; Chen, C.; Liu, C.; Wang, S. Study on Porous Mg-Zn-Zr ZK61 Alloys Produced by Laser Additive Manufacturing. *Metals* **2018**, 8(8), 635. https://doi.org/10.3390/met8080635
32. Liu, C.; Zhang, M.; Chen, C. Effect of laser processing parameters on porosity, microstructure and mechanical properties of porous Mg-Ca alloys produced by laser additive manufacturing. *Mater. Sci. Eng. A* **2017**, *703*, 359–371
33. Bita T., Corneschi I., Ungureanu E., Bita A.I., Ignat N.D., Dura H., Carstoc I.D., Nicolcescu P., Influence of heat treatment on microstructure and corrosion behavior of biodegradable Mg-Ca alloy, *U.P.B. Sci. Bull., Series B*, **2023**, 85(4), https://www.scientificbulletin.upb.ro/rev_docs_arhiva/full9d8_327223.pdf
34. N. Ikeo, M. Nishioka, T. Mukai, Fabrication of biodegradable materials with high strength by grain refinement of Mg–0.3 %at. Ca alloys, *Materials Letters*, **2018**, 223, 65-68.
35. M. Deng, L. Wang, D. Snihirova, J. Bohlen, G. Kurz, S.V. Lamaka, D. Höche, M.L. Zheludkevich, Micro-alloyed Mg-Ca: Corrosion susceptibility to heating history and a plain problem-solving approach, *J. Magnes. Alloys*, **2023**, 11(4), 1193-1205.
36. J. Wang, J. Dou, Z. Wang, C. Hu, H. Yu, C. Chen, Research progress of biodegradable magnesium-based biomedical materials: A review, *Journal of Alloys and Compounds*, Vol. 923, **2022**, https://doi.org/10.1016/j.jallcom.2022.166377.

37. H.L. Ding, P. Zhang, G.P. Cheng, S. Kamado, Effect of Ca addition on the microstructure and creep behaviour of AZ91 Mg alloy, *Materials Today: Proceedings*, online 16 March **2023**, https://doi.org/10.1016/j.matpr.2023.03.056.
38. L. Shi, S. Chen, F. Zheng, M. Liu, H. Yang, B. Zhang, Corrosion resistance evaluation of biodegradable magnesium alloy vascular stents optimized by mechanical adapted polymer coating strategy, *Colloids and Surfaces A: Physicochemical and Engineering Aspects*, 658, 5 February **2023**, 130664, https://doi.org/10.1016/j.colsurfa.2022.130664
39. Nowosielski, R.; Gawlas-Mucha, A.; Borowski, A.; Guwer, A.; Fabrication and properties of magnesium based alloys Mg-Ca, *JAMME*, **2013** (21), 61(2):367-374
40. Shuai, C.; Yang, Y.; Wu, P.; Lin, X.; Liu, Y.; Zhou, Y.; Feng, P.; Liu, X.; Peng, S. Laser rapid solidification improves corrosion behavior of Mg-Zn-Zr alloy. *J. Alloys Compd*. **2017**, 691, 961–969.
41. Nayeb-Hashemi, A.A., Clark, J.B. The Mg–Zr (Magnesium-Zirconium) system. *Bulletin of Alloy Phase Diagrams,* **1985**, 6, 246–250; https://doi.org/10.1007/BF02880408
42. Manic, M., Vitković, N., Mitic, J. (**2022**). Design and Manufacturing of the Personalized Plate Implants. In: Canciglieri Junior, O., Trajanovic, M.D. (eds) *Personalized Orthopedics*. Springer, Cham. https://doi.org/10.1007/978-3-030-98279-9_6
43. Jariwala, S.H.; Lewis, G.S.; Bushman, Z.J.; Adair, J.H.; Donahue, H.J. 3D printing of personalized artificial bone scaffolds. *3D Print. Addit. Manuf.* **2015**, 2, 56–64.
44. Nopová, K.; Jaroš, J.; Cervinek, O.; Pantˇelejev, L.; Gneiger, S.; Senck, S.; Koutný, D. Processing of AZ91D Magnesium Alloy by Laser Powder Bed Fusion. *Appl. Sci.* **2023**, 13, 1377.
45. Yang, Y.; Ping, W.; Xin, L.; Yong, L.; Hong, B.; Zhou, Y.; Gao, C.; Shuai, C. System development, formability quality and microstructure evolution of selective laser-melted magnesium. *Virtual Phys. Prototyp*. **2016**, 11, 173–181.
46. Chen, L.; Lin, Z.; Wang, M.; Huang, W.; Ke, J.; Zhao, D.; Yin, Q.; Zhang, Y. Treatment of trauma-induced femoral head necrosis with biodegradable pure Mg screw-fixed pedicle iliac bone flap. *J. Orthop. Transl*. **2019**, 17, 133–137
47. Karunakaran ROrtgies, S.; Tamayol, A.; Bobaru, F.; Sealy, M.P. Additive manufacturing of magnesium alloys. *Bioact. Mater.* **2020**, 5, 44–54.
48. Hassan, S.F.; Islam, M.T.; Saheb, N.; Baig, M.M.A. Magnesium for Implants: A Review on the Effect of Alloying Elements on Biocompatibility and Properties. *Materials* **2022**, 15, 5669.
49. Chen, J.; Xu, Y.; Kolawole, S.K.; Wang, J.; Su, X.; Tan, L.; Yang, K. Systems, Properties, Surface Modification and Applications of Biodegradable Magnesium-Based Alloys: A Review. *Materials* **2022**, 15, 5031.
50. Zhao, D.; Witte, F.; Lu, F.; Wang, J.; Li, J.; Qin, L. Current status on clinical applications of magnesium-based orthopaedic implants: A review from clinical translational perspective. *Biomaterials* **2017**, 112, 287–302
51. Lesz, S.; Hrapkowicz, B.; Karolus, M.; Gołombek, K. Characteristics of the Mg-Zn-Ca-Gd Alloy after Mechanical Alloying. *Materials* **2021**, 14, 226.
52. Salleh, E.M.; Ramakrishnan, S.; Hussain, Z. Synthesis of Biodegradable Mg-Zn Alloy by Mechanical Alloying: Effect of Milling Time. *Procedia Chem.* **2016**, 19, 525–530.
53. Abbasi, M.; Sajjadi, S.A.; Azadbeh, M. An investigation on the variations occurring during Ni3Al powder formation by mechanical alloying technique. *J. Alloys Compd*. **2010**, 497, 171–175.
54. Raducanu, D.; Cojocaru, V.D.; Nocivin, A.; Hendea, R.E.; Ivanescu, S.; Stanciu, D.; Trisca-Rusu, C.; Serban, N.; Drob, S.I.; Campian, R.S. *Microstructure Evolution during Mechanical Alloying of a Biodegradable Magnesium Alloy*. **Crystals 2022**, 12(11), 1641. https://doi.org/10.3390/cryst12111641
55. Hendea R.E., Raducanu D., Nocivin A., Ivanescu S., Stanciu D., Trisca-Rusu C., Campian R.S., Drob S.I., Cojocaru V.D., Gălbinasu B.M., *Laser Powder Bed Fusion Applied to a New Biodegradable Mg-Zn-Zr-Ca Alloy*, **Materials 2022**, 15(7), 2561. https://doi.org/10.3390/ma15072561
56. K. Park, B.Y. Chang, and S. Hwang, Correlation between Tafel Analysis and Electrochemical Impedance Spectroscopy by Prediction of Amperometric Response from EIS, *ACS Omega* **2019**, *4*(21), 19307-19313; https://doi.org/10.1021/acsomega.9b02672
57. Suryanarayana C., Mechanical Alloying: A Novel Technique to Synthesize Advanced Materials, *Research* **2019**, Article ID 4219812, 17 p., https://doi.org/10.34133/2019/4219812
58. Lesz, S.; Hrapkowicz, B.; Karolus, M.; Gołombek, K. Characteristics of the Mg-Zn-Ca-Gd Alloy after Mechanical Alloying. *Materials* **2021**, 14, 226. https://doi.org/10.3390/ma14010226
59. M. Lichtenauer, S. Nickl, K. Hoetzenecker, A. Mangold, B. Moser, M. Zimmermann, S. Hacker, T. Niederpold, A. Mitterbauer, H. J. Ankersmit, Phosphate Buffered Saline Containing Calcium and Magnesium Elicits Increased Secretion of Interleukin-1 Receptor Antagonist, *Laboratory Medicine*, **2009**, 40(5), 290–293; https://doi.org/10.1309/LMBMG5A7NOVQBXWD
60. Ouyang, Y.; Chen, Z.; Jiang, C.; Yang, W.; Chen, Y.; Yin, X.; Liu, Y. Design of the double-layer biocompatible coating on AZ31 magnesium alloy for highly effective corrosion resistance. *Surf. Coat. Technol*. **2021**, 428, 127897.

 doi:10.20944/preprints202403.0813.v1

61. Ma, E. Alloys created between immiscible metals. *Prog. Mater. Sci*. **2005**, 50, 413–509.
62. Suryanarayana, C.; Liu, J. Processing and characterization of mechanically alloyed immiscible metals. *Int. J. Mater. Res.* **2012**, 103, 1125–1129.
63. Fu, W.; Yang, H.; Li, T.; Sun, J.; Guo, S.; Fang, D.; Qin, W.; Ding, X.; Gao, Y.; Sun, J. Enhancing corrosion resistance of ZK60 magnesium alloys via Ca microalloying: The impact of nanoscale precipitates. *J. Magnes. Alloys* **2023**, 11(9), 3214-3230. https://doi.org/10.1016/j.jma.2022.06.011
64. Biancardi, O.V.; Luccas Rosa, V.; de Abreu, L.B.; Tavares, A.P.R.; Corrêa, R.G.; Cavalcanti, P.H.; Napoleão, B.I.; da Silva, E.P. Corrosion behavior of as-cast ZK60 alloy modified with rare earth addition in sodium sulfate medium. *Corros. Sci*. **2019**, 158, 108092.
65. Mandal, M.; Mondal, K. Effect of Micro-alloying and Microstructure on the Corrosion Behavior of As-Cast Mg-6.2 wt.% Zn Alloy. *J. Mater. Eng. Perform*. **2020**, 29, 6691–6700.
66. Xue, Y.; Pang, X.; Karparvarfard, S.M.H.; Jahed, H.; Luo, S.; Shen, Y. Corrosion Protection of ZK60 Wrought Magnesium Alloys by Micro-Arc Oxidation. *Metals* **2022**, 12, 449.
67. Merson, D.; Vasiliev, E.; Markushev, M.; Vinogradov, A. On the corrosion of ZK60 magnesium alloy after severe plastic deformation. *Lett. Mater.* **2017**, 7, 421–427.
68. Merson, E.; Poluyanov, V.; Myagkikh, P.; Merson, D.; Vinogradov, A. Fractographic features of technically pure magnesium, AZ31 and ZK60 alloys subjected to stress corrosion cracking. *Mater. Sci. Eng. A*, **2020**, 772, 138744.
69. Hassan, H.W.; Rahmati, M.; Barrantes, A.; Haugen, H.J.; Mirtaheri, P. In Vitro Monitoring of Magnesium-Based Implants Degradation by Surface Analysis and Optical Spectroscopy; *Int. J. Mol. Sci*. **2022**, 23, 6099; https://doi.org/10.3390/ijms23116099